Residual migration

Daniel Rothman, Stewart Levin, and Fabio Rocca

Abstract

Rocca and Salvador (1982) showed that migration velocity can be modified by applying a residual migration to previously migrated data, rather than having to remigrate the original data with the corrected velocity field. The effective velocity entering this residual processing is usually small compared to the original migration velocity. This decreases computational cost compared to a full migration, and allows the initial migration to be done with a less accurate but faster algorithm than would otherwise be required.

The possible advantages are many. The overall cost of migration may be reduced, a consideration especially important when migrating 3-D datasets. Migration quality may also be improved, both from the corrected location of mispositioned reflectors and the freedom to initially migrate with a high dip, low dispersion algorithm such as Stolt migration. Interactive residual sharpening of the migrated image also becomes feasible.

The theoretical and practical limitations of residual migration are discussed. The related reductions of effective dip, velocity, and frequency after initial migration are quantified. We determine how accurate the initial migration velocity needs to be to justify use of this approach. Aliasing and numerical artifacts are also analyzed. Field data examples using Kirchhoff summation migration are shown to illustrate the features and drawbacks of the method.

Introduction

Residual migration is based upon the observation, made by Rocca and Salvador (1982) and others (Larner, private communication), that migration with velocity v_1 followed by migration with velocity v_2 is equivalent to migration with a combined velocity $v = \sqrt{v_1^2 + v_2^2}$. By viewing v as the proper migration velocity and v_m as the migration velocity

actually used, Rocca and Salvador solved for the residual migration velocity $v_\varepsilon = \sqrt{v^2 - v_m^2}$ needed to effect correct migration.

This ability to correct for improper migration velocity has two important consequences. First, because the residual velocity is generally small, remigration with an adjusted velocity function can be done at a fraction of the cost of a full migration, making, for example, interactive sharpening and focusing of the migrated image feasible. Second, it provides a means of correcting for the inherent constant velocity nature of Stolt migration, permitting wider use of its steep dip accuracy and low dispersion, possibly at less total cost than full migration with more flexible finite difference or Kirchhoff methods. The savings gained by residual migration would be most substantial in 3-D processing: 3-D migration could first be performed with a Stolt algorithm, followed by residual corrections.

To examine the limitations of a residual migration scheme, we look at how effective dip varies with velocity error and how the frequency downshift from an initial migration affects the cost and quality of a subsequent migration. We see that dip and frequency downshift control the critical choices of finite difference depth step or Kirchhoff aperture sampling for the residual migration. In the case of residual Kirchhoff migration, we show that the problems of aliasing and undersampling of the residual summation operator are no worse than we are accustomed to in ordinary Kirchhoff migration, despite the steep (low velocity) flanks of diffraction hyperbolas. Finally, a field data example is presented.

Geometric view of residual migration

The process of migration can be thought of as mapping apparent dip $\frac{dt}{dx}$ to a true dip $\frac{d\tau}{dx}$ via the relations

$$\sin\theta = \frac{v}{2}\,\frac{dt}{dx} \tag{1a}$$

$$\tan\theta = \frac{v}{2}\,\frac{d\tau}{dx} \tag{1b}$$

which yield, when θ is eliminated, the classic formula

$$\frac{d\tau}{dx} = \frac{dt}{dx}\left[1 - \left(\frac{v}{2}\,\frac{dt}{dx}\right)^2\right]^{-1/2} \tag{2}$$

expressing time dip on the migrated section in terms of the time dip on the unmigrated data. If the migrated section described by equation (2) is then input to another migration using velocity v', the formula now yields the new migrated slope

$$\frac{d\tau'}{dx} = \frac{d\tau}{dx}\left[1 - \left(\frac{v'}{2}\frac{d\tau}{dx}\right)^2\right]^{-1/2}$$

$$= \frac{dt}{dx}\left[1 - \frac{v^2 + v'^2}{4}\left(\frac{dt}{dx}\right)^2\right]^{-1/2} \tag{3}$$

which is (2) with v replaced by $\sqrt{v^2 + v'^2}$, exactly as predicted by Rocca and Salvador.

Suppose now that the initial migration velocity v_m is in error and that the true velocity is v. Then solving for v' demonstrates that to transform this improperly migrated data to correctly migrated data requires migration with a new *residual velocity*

$$v_\varepsilon = v\left[1 - \left(\frac{v_m}{v}\right)^2\right]^{1/2} \qquad \text{when } v_m < v \tag{4a}$$

or modeling (i.e., unmigrating) with

$$v_\varepsilon = v\left[\left(\frac{v_m}{v}\right)^2 - 1\right]^{1/2} \qquad \text{when } v_m > v \quad . \tag{4b}$$

A more general derivation of the residual velocity v_ε is provided in the Appendix, where we show that if v is a depth-variable function $v(z)$, then a residual velocity, $v_\varepsilon(z)$, also varying with depth, will correct for a preliminary migration performed with constant velocity. This statement is wave-theoretically precise: low velocity diffractions present after migration with $v_m < v$ are still diffractions in the ordinary sense. The amplitude and phase variations expected for pre-migration diffractions still exist. For the case $v_m > v$, we would observe elliptical "smiles." Residual migration would then be performed by modeling, still a wave-theoretically valid procedure.

For the case of constant velocity, it is interesting to note that one derivation of the residual migration velocity closely parallels the proof that 3-D migration can be split into two, perpendicular passes of 2-D migration (Jakubowicz and Levin, 1983). Indeed, residual migration can be derived as a special case by the following argument.

Suppose seismic data are collected over a two dimensional subsurface. If $P_0(x,t)$ denotes the stacked section that would be obtained along a dip line, we would get $P(x,y,t) = P_0(x\cos\varphi + y\sin\varphi, t)$ if the survey were shot along an azimuth φ, or, expressed differently, we would see the same traces spaced farther apart. (On a strike line, $\varphi = 90°$, they would be infinitely far apart.) Two-pass migration with velocity v is equivalent to migrating $P_0(x,t)$ twice; first with velocity $v\cos\varphi$ followed by velocity $v\sin\varphi$. Indeed, in the frequency-wavenumber domain, a component sinusoid with frequency ω and wavenumber k has projections $k_x = k\cos\varphi$ and $k_y = k\sin\varphi$ in the inline and crossline directions

respectively. Migrating in the inline direction replaces ω by

$$\hat{\omega} = \left(\omega^2 - (\tfrac{1}{2} v\, k_x)^2\right)^{1/2} , \tag{5}$$

the same as migrating with velocity $v\cos\varphi$. Remigrating in the crossline direction produces

$$k_\tau = \left(\hat{\omega}^2 - (\tfrac{1}{2} v\, k_y)^2\right)^{1/2} , \tag{6}$$

the same as remigrating with velocity $v\sin\varphi$.

Thus we may interpret (under)migration with the wrong velocity as equivalent to migrating, using the correct velocity, data from lines at some azimuth away from the dip direction. Residual migration completes the job by performing the missing crossline migration.

This geometric visualization is important - no longer do we need to work within the uncharted territory of velocities outside the normal range used in migration. We may, instead, view residual migration as migration with a stretched spatial axis and our original velocity. Then almost all of our experience and intuition about migration, both its strengths and its limitations, can be safely brought to bear on this problem.

Reduction of effective dip

A preliminary migration changes the effective velocity of the data, which in turn alters the apparent dip which remains to be migrated. The range of dip which can be correctly migrated depends on the particular algorithm chosen. In Kirchhoff migration, for example, the lateral extent (aperture width) of the summation operator determines the maximum dip migrated. Alternatively, finite difference algorithms are designed to be accurate within a specific range of dip, usually 15 or 45 degrees. Generally, the higher the dip, the more expensive the algorithm. Since one goal of residual migration is to reduce the expense of migration by doing most of the work with a preliminary, rapid Stolt migration, it is beneficial to know when the effective residual dip is small enough to be properly handled by a low order residual migration algorithm.

After initial migration with velocity v_m, the apparent dip input to a residual migration can be determined by combining $\frac{d\tau}{dx}$ in equation (2) with equations (1a,b). The effective *residual dip* θ_e is then given by

$$\tan\theta_e = \tan\theta \left[1 - \left(\frac{v_m}{v}\right)^2 \right]^{1/2} \qquad v_m < v \tag{7a}$$

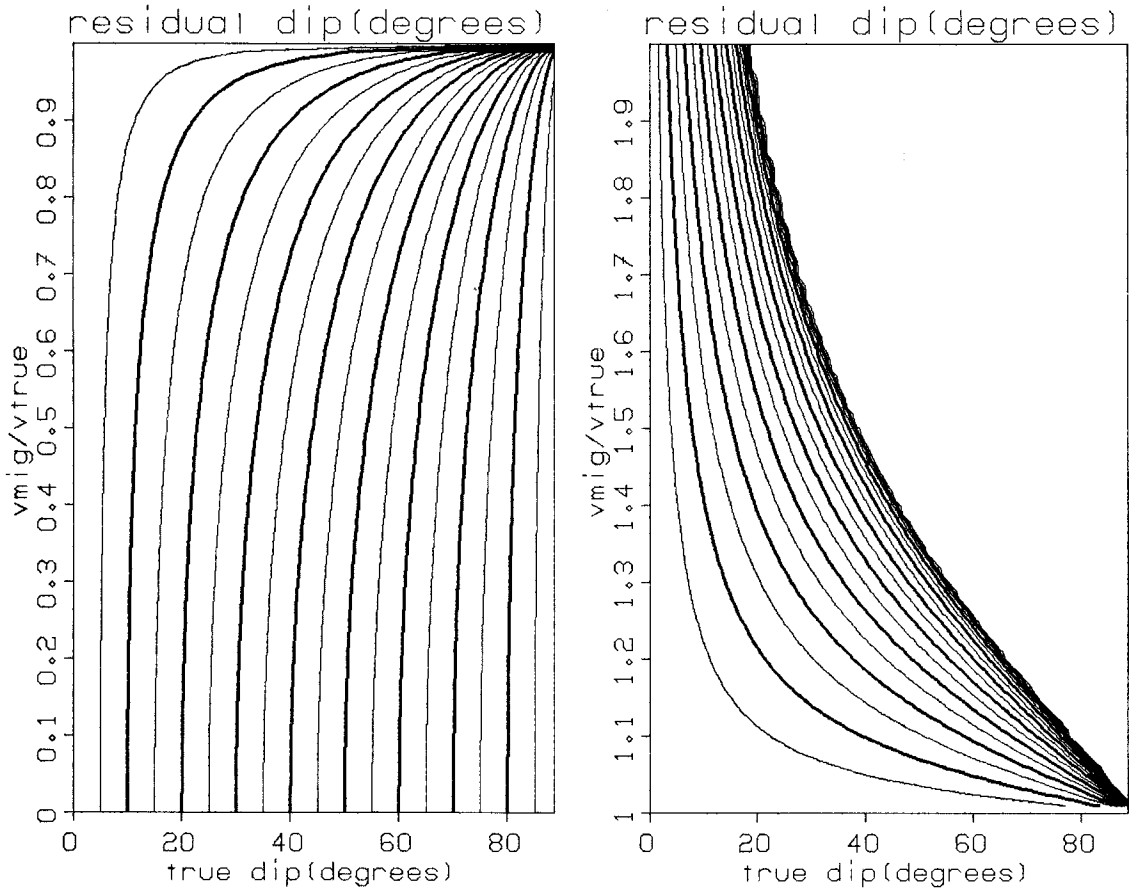

FIG. 1. Contours of residual dip as a function of initial migration velocity accuracy and true dip. $v_m < v$ on the left, and $v_m > v$ on the right. Contours range from 5° to 85°, left to right, on both plots. For example, 30° dip is reduced to 15° when initially migrated at 90% of the proper velocity. Notice also the large empty space in the second figure where data is treated as evanescent energy in the initial overmigration.

$$\sin \theta_\varepsilon = \tan \theta \left[\left(\frac{v_m}{v} \right)^2 - 1 \right]^{1/2} \qquad v_m > v \ . \tag{7b}$$

Both cases are contoured in Figure 1. From this pair of formulas we can bracket the range of initial migration velocities that reduce the effective dip by solving for $\theta_\varepsilon = \theta$ to get

$$0 \le v_m \le v \sqrt{1 + \cos^2 \theta} \ . \tag{8}$$

This agrees with common wisdom: undermigration still moves events closer to where they should migrate, but overmigration can be worse than no migration at all. If v_m is substantially greater than v, we not only risk increasing the remaining dip to be migrated, but much data may be lost due to its treatment as evanescent energy. Figure 1 tell us even more: our

first migration velocity needs to be within 10% of the correct velocity to yield any significant decrease in dip.

Finite difference residual migration

Reduced velocity and decreased dip are not the only benefits gained from a preliminary migration. In addition, recall that migration decreases the frequency of dipping beds according to the formula

$$\omega_m = \omega \cos\theta \ . \tag{9}$$

This frequency downshift also provides a savings for residual migration.

Finite difference migration consists of extrapolating the unmigrated stacked section downward into the earth to image the reflection structure of the subsurface. The actual imaging is done by concatenating small strips of successively deepened time sections. Savings in migration cost are gained by increasing the width of these strips and taking the largest extrapolation steps commensurate with numerical accuracy. Accuracy is essentially controlled by making the step size some appropriately small fraction of the wavelength of variation in the direction of extrapolation. This wavelength depends, in turn, on the dip and frequency of the data to be extrapolated.

Suppose that we have a plane dipping event with subsurface dip θ and frequency ω. Then, in the retarded coordinate frame in which we extrapolate, the frequency of variation in migrated traveltime τ is given by

$$k'_\tau = \omega \cos\theta - \omega \ , \tag{10a}$$

or, in the case of modeling,

$$\omega' = k_\tau \sec\theta - k_\tau \ . \tag{10b}$$

Thus there is no variation for flat reflectors, but the variation does increase with dip, and in (10a) is equal to the input frequency at 90°. The wavelength is, of course, inversely proportional to frequency. After preliminary migration we have seen that both the effective frequency and dip in equation (9) will change. Defining β, the ratio of the cosine of the apparent dip after the first migration to the cosine of the true dip, by

$$\beta \cos\theta = \left[1 - \left[\frac{v_m}{v}\sin\theta\right]^2\right]^{1/2} \ , \tag{11}$$

the new values for frequency and dip, derived from equations (7) and (9), are

$$\omega_\varepsilon = \omega \beta \cos\theta \qquad v_m < v \tag{12a}$$

$$k_{\tau_\varepsilon} = \omega \beta \cos\theta \qquad v_m > v \tag{12b}$$

and

$$\cos\theta_\varepsilon = \beta^{-1} \qquad v_m < v \tag{13a}$$

$$\sec\theta_\varepsilon = \beta^{-1} \qquad v_m > v \ . \tag{13b}$$

The frequency of variation in the retarded coordinate frame is thus computed to be

$$k'_{\tau_\varepsilon} = \omega \cos\theta (1 - \beta) \qquad v_m < v \tag{14a}$$

$$\omega'_\varepsilon = \omega \cos\theta (1 - \beta) \qquad v_m > v \ . \tag{14b}$$

Figure 2 compares this with the unmigrated k'_τ of equation (8) and shows a much less bleak picture than our plots of effective dip. We now find that even as much as a 30% velocity error will still permit double the step size needed for unmigrated data. This approximately halves the expense of a finite difference residual migration, making it cost effective when used with a rapid initial migration algorithm.

Residual migration by Kirchhoff summation

The decrease in effective dip and velocity caused by a preliminary migration are reflected as a substantial reduction in the aperture needed by a subsequent residual Kirchhoff migration. Recall that Kirchhoff migration involves a weighted summation along a hyperbolic path. The lateral extent of this summation, the aperture, is adjusted to encompass all the dip of interest. In general, the aperture half-width L is given by

$$L = \frac{v}{2} \tau \tan\theta \qquad \text{for migration ,} \tag{15a}$$

$$L = \frac{v}{2} \tau \sin\theta \qquad \text{for modeling .} \tag{15b}$$

The substitution of v_ε for v [from equations (4a,b)] and θ_ε for θ [from equations (7a,b)]

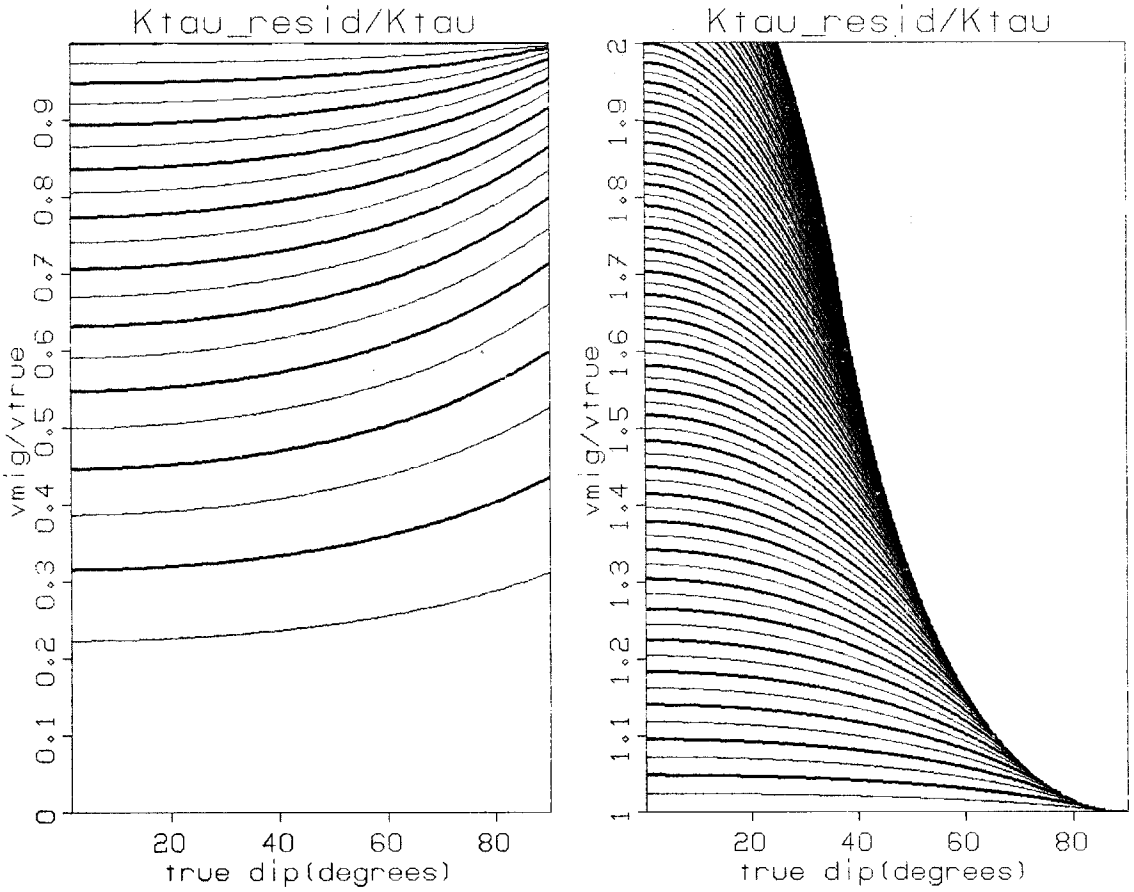

FIG. 2. Change in residual migration extrapolation wavenumber as a function of initial migration velocity accuracy and true dip. Contours represent the ratio $k'_{\tau_\varepsilon} / k'_\tau$, ranging from 5% to 95%, top to bottom, on the left, and increasing from 5% to infinity, bottom to top, on the right. For example, at 40° dip, extrapolation wavenumber is decreased fivefold when initialiy migrated at 90% of the proper velocity.

yields the required aperture for residual migration,

$$L_\varepsilon = \begin{cases} \dfrac{v}{2}\tau \tan\theta \left[1 - \left(\dfrac{v_m}{v} \right)^2 \right] & v_m < v \\ \dfrac{v}{2}\tau \tan\theta \left[\left(\dfrac{v_m}{v} \right)^2 - 1 \right] & v_m > v \end{cases} . \tag{16}$$

We see that L_ε differs from L by the square of the relative velocity error. The ratio L_ε/L is plotted in Figure 3 as a function of v_m/v ; it measures a savings gained by a residual Kirchhoff migration compared with the same operation on unmigrated data. For example, one sees that undermigration by 30% reduces the aperture (and the computational work) for a

residual Kirchhoff migration by approximately half. Comparison of Figures 2 and 3 shows that the savings accrued by both finite difference and Kirchhoff implementations of residual migration are quite similar. The Kirchhoff method, however, provides more flexibility in local enhancement of small portions of previously migrated data, a particularly important consideration in 3-D processing.

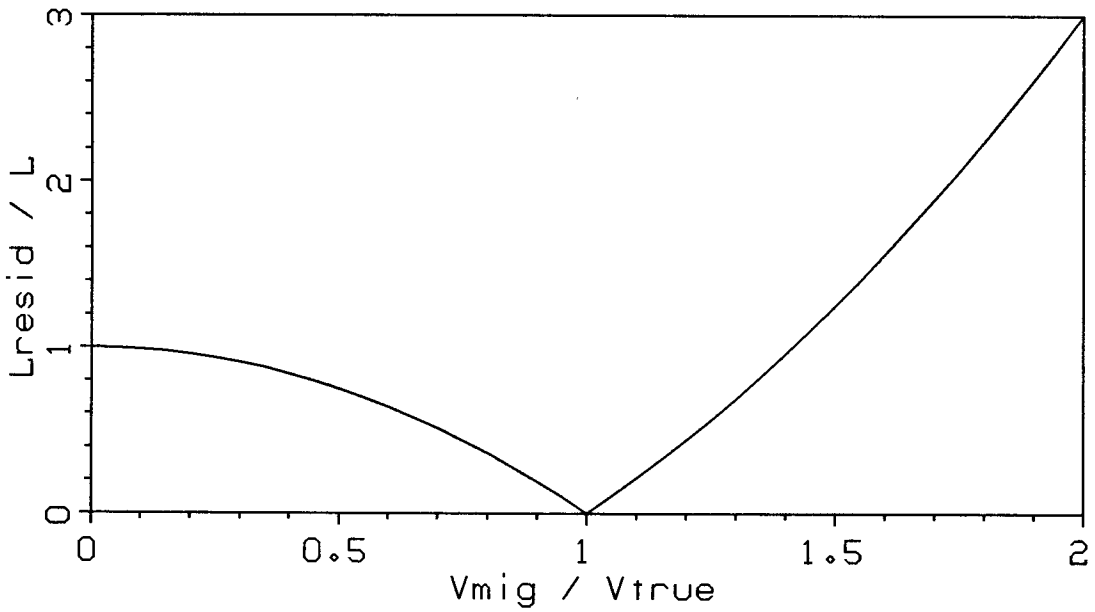

FIG. 3. Change in aperture width as a function of the accuracy of the initial migration velocity. For example, a 10% error in velocity decreases the necessary migration aperture by about 80%.

Aliasing of the residual Kirchhoff operator

A pervasive problem in Kirchhoff migration is aliasing noise. This commonly occurs when migrating shallow reflections, because relatively high frequency data and steeply dipping, low velocity hyperbolic summation paths combine to cause spatial aliasing. The slow velocities used in residual migration might lead one to expect a more severe aliasing problem; fortunately, we now show, this is not the case.

The Kirchhoff operator in a residual migration follows a summation path described by

$$\tau_\varepsilon = \begin{cases} \left[\tau^2 + \dfrac{4x^2}{v_\varepsilon^2}\right]^{1/2} & v_m < v \\ \\ \left[\tau^2 - \dfrac{4x^2}{v_\varepsilon^2}\right]^{1/2} & v_m > v \end{cases} , \tag{17}$$

where τ is the correct migrated travel time (either the apex of a hyperbola or the base of an ellipse), and τ_ε and x denote time and offset on the residual summation path. At any given point on the path the slope is given by the derivative,

$$\frac{d\tau_\varepsilon}{dx} = \frac{\pm 4x}{v_\varepsilon^2 \tau_\varepsilon} . \tag{18}$$

The $\pm$ refers to those of equation (17). At $x = L_\varepsilon$, the edge of the aperture defined in equation (16), we obtain the residual migration operator's maximum slope,

$$m_\varepsilon \equiv \left[\frac{d\tau_\varepsilon}{dx}\right]_{x=L_\varepsilon} = \frac{\pm 2\tan\theta}{\beta v} , \tag{19}$$

with β again defined by equation (11). Aliasing occurs if the maximum wavenumber to be migrated is greater than the Nyquist wavenumber determined by the spatial sampling interval. Wavenumber is the product of frequency and slope, so, for residual migration, the maximum wavenumber $\hat{k}_\varepsilon$ is given by

$$\hat{k}_\varepsilon = \hat{\omega}_\varepsilon m_\varepsilon , \tag{20}$$

where $\hat{\omega}_\varepsilon$ represents the highest frequency present after the preliminary migration. For a full migration, the operator's steepest trajectory is given by the largest slope on the unmigrated section; thus, from equation (1a),

$$m \equiv \left[\frac{dt}{dx}\right]_{x=L} = \frac{2\sin\theta}{v} . \tag{21}$$

The maximum wavenumber before migration is $\hat{k} = \hat{\omega} m$. From (12), $\hat{\omega}_\varepsilon = \hat{\omega}\beta\cos\theta$, and we find the simple relations

$$\hat{\omega} m = \hat{\omega}_\varepsilon m_\varepsilon \tag{22a}$$

$$\hat{k} = \hat{k}_\varepsilon . \tag{22b}$$

Thus the maximum wavenumber to be migrated is no higher for residual migration than it is for

ordinary, full migration. Although the slope of the Kirchhoff operator is steeper for a residual migration, the accuracy of the 2-dimensional sampling performed by the residual operator is effectively the same as that of a full Kirchhoff operator - the frequency downshift resulting from the first migration counterbalances the increase in slope. This confirms what we already know from the Stolt mapping of equation (9): accurate migration alters slope, but leaves wavenumber unchanged. For this reason, aliasing is no more of a problem for residual Kirchhoff migration than it is for any Kirchhoff migration. This underscores the theoretic equivalence of residual migration to full remigration.

Another, related problem that occurs in Kirchhoff migration results from the hyperbolic moveout corrections performed prior to summation. This differential time shift, or NMO stretch, varies inversely with velocity. Stretch must be limited to prevent high frequency attenuation and other related degradations. Fortunately, stretch is even *less* of a problem for residual Kirchhoff migration than it is normally.

For a residual migration with constant v_ε, stretch is defined as the change of apex (migrated) time with respect to flank (unmigrated) time which, in terms of the summation paths of (17), is given by

$$\frac{d\tau}{d\tau_\varepsilon} = \left[1 \pm \frac{4x^2}{\tau^2 v_\varepsilon^2}\right]^{1/2} . \tag{23}$$

Substituting L_ε for x once again, we find the maximum stretch for residual migration,

$$\left[\frac{d\tau}{d\tau_\varepsilon}\right]_{x=L_\varepsilon} = \beta . \tag{24}$$

Referring back to β in equation (11), we can see that stretch for a residual migration decreases as the initial migration velocity becomes more accurate. This emphasizes that residual migration (ideally) performs only a minor operation on data.

Finally, dividing equation (19) by (21) yields the elegant relation

$$\frac{d\tau_\varepsilon}{dt} = \frac{\omega}{\omega_\varepsilon} \tag{25}$$

between NMO stretch in Kirchhoff migration and the frequency downshift of migrated dips, reconciling both wave- and ray-theoretical views of migration.

Implementing residual Kirchhoff migration

We have chosen to use a Kirchhoff diffraction-summation algorithm for the residual migrations illustrated in this report. The choice is practical: a Kirchhoff algorithm allows local remigration of an arbitrarily small subset of previously migrated data, and has no causality (stability) problems when crossing a zero of the residual velocity function. Finite difference algorithms, though adaptable to this problem, demand more conventional input, being less conducive to small, sectional enhancement. The remaining alternative, frequency domain algorithms, are the least efficient for a residual task - no savings are gained whatsoever.

Any Kirchhoff algorithm normally used should be capable of residual migration. We have found it necessary, however, to make some minor, but important, adjustments to avoid numerical problems. These occur when the initial migration velocity is nearly equal to the true velocity, leaving a residual migration aperture as little as 1 or 2 traces wide, or even less. Two problems then become apparent. The first is cosmetic - residually migrated data may contain noticeably unattractive computational artifacts where the aperture change is large in proportion to its size; for example, where the aperture radius increases from 1 to 2 traces. The second, related problem is fundamental to the accuracy of residual Kirchhoff migration. Kirchhoff algorithms essentially perform numerical integration over hyperbolic paths. The accuracy of this integration (or, indeed, of migration in general) is directly affected by the trace spacing (Larner, Gibson, and Rothman, 1980). Recalling the geometric view of residual migration described earlier, and the traveltime curve for a residual diffraction,

$$\tau_\varepsilon^2 = \tau^2 + \frac{4x^2}{v^2\left[1 - \left(\frac{v_m}{v}\right)^2\right]} \quad , \tag{26}$$

we note that the factor in brackets may just as easily be thought to modify x instead of v. Residual migration would then be conducted with the same velocity, but with the new, wider trace spacing

$$\Delta x' = \Delta x\left[1 - \left(\frac{v_m}{v}\right)^2\right]^{-1/2} \quad . \tag{27}$$

Aliasing, as we have shown, is still no more of a problem than it was previously. But the stretched spatial axis does indicate the coarseness of the numerical integration that is performed. We have chosen to ensure numerical accuracy by spatial interpolation, decreasing $\Delta x'$ to its original width, Δx. This does limit the savings gained by a residual Kirchhoff migration, but, if strictly applied, still results in an aperture reduction by a factor of $[1-(v_m/v)^2]^{1/2}$ [see equation (16)]. Numerical accuracy does not solely hinge upon this

square root factor, however, and is in practice largely dependent upon the range of spatial and temporal frequencies in the data. We note that explicit trace interpolation is not necessary; more sophisticated numerical integration schemes are based on coefficients obtained by analytically integrating interpolated data. These methods have not yet been implemented, however.

When velocity is not constant

When the first migration is performed with non-constant velocity, residual migration, much like two-pass 3-D migration, is not exact. Consider a point diffractor between two layers with velocity v_1 in the upper layer and v_2 in the lower. The time section would be an hyperbola characterized by the velocity v_1 of the upper medium. If we now migrate it with velocity v_1 in layer 1 and zero in layer 2 for our first pass, the diffraction collapses nicely to a point. A second pass with zero velocity in the first layer and v_2 in the second leaves this picture unchanged - a perfect migration. Reversing the order we have quite a different story - the first migration will do *something* to the diffractor which in turn insures that the second migration cannot collapse it to a point.

We can even make the stronger statement that *no* velocity is correct for the second migration. We can see this by calculating where the initial hyperbola

$$t^2 = t_o^2 + \frac{4x^2}{v_1^2} \tag{28}$$

is migrated using the summation paths

$$(t - t_o)^2 = (\tau - t_o)^2 + \frac{4y^2}{v_2^2} \quad . \tag{29}$$

This can be done by equating dt/dx with dt/dy from equations (28) and (29) to find the points of tangency and the corresponding apex time τ and offset $z = x - y$ to which energy migrates. Thus we solve the simultaneous equations

$$\begin{aligned} v_1^2\, t\, \frac{dt}{dx} &= 4x \\ v_2^2\, (t - t_o)\, \frac{dt}{dx} &= 4y \end{aligned} \tag{30}$$

for y and substitute in equations (28) and (29) to find the resulting curve described parametrically by

$$\begin{aligned} \frac{z^2}{v_1^2} &= (t^2 - t_o^2) \left[1 - \frac{v_2^2}{v_1^2}\, \frac{(t - t_o)}{t} \right]^2 \\ (\tau - t_o)^2 &= (t - t_o)^2 \left[1 - \frac{v_2^2}{v_1^2}\, \frac{(t^2 - t_o^2)}{t^2} \right] \end{aligned} \quad . \tag{31}$$

In the case $v_1 = v_2$ we can solve explicitly and get

$$\frac{z^2}{v_1^2} = \frac{(\tau - t_o)^3}{3t_o - \tau} \tag{32}$$

which is neither an hyperbola nor an ellipse. No summation path, hyperbolic or elliptical, can collapse this to the correct position.

That the first order of migration did properly migrate can be generalized to the statement that a constant velocity migration can be followed by a depth variable residual migration to achieve the same effect as a full depth variable migration. A straightforward proof of this is presented in the Appendix.

Field data example

Figure 4 displays a zero-offset, unmigrated, stacked section of data from the Gulf of Mexico. Dip moveout (Hale, 1982) has been applied prior to stacking. The traces are spaced 33m apart, and the temporal sampling interval is 8 msec. The true migration velocities range from 1650 m/sec to 2000 m/sec. The steepest dips on the section, the fault plane reflections, are between 30 and 40 degrees.

Figure 5 shows the same data after a constant velocity Stolt migration with v_m = 1600 m/sec. For these data, correct migration velocities are those which most accurately place the fault plane reflections in their proper positions - at the bed truncations demarcating the growth faults. Velocities here vary both laterally and with depth; evidence of the lateral variation is seen by observing the fault reflection beginning at about trace 100, which is further from its proper position than the other major fault reflections on the section. This indicates that it emanates from a different azimuth relative to the other major fault reflections in the data, and needs an artificially high velocity to be correctly migrated.

Figure 6 displays the residual migration, using our Kirchhoff algorithm, of the data in Figure 5. The fault plane reflections, slightly mispositioned before, have now migrated to their correct locations. The aperture half-width of this migration ranged from 1 trace at the top of the section to 17 traces at the bottom. Due to the very small residual velocities at early times, traces were interpolated to 4 times the actual trace spacing prior to summation along diffraction paths. Although this degree of interpolation was only necessary for the shallowest data, programming considerations made this the most expedient (but not necessarily computationally efficient) choice for the entire section.

Figure 7 exhibits the full Kirchhoff migration of the original, unmigrated data in Figure 4. The aperture width used here ranged from 17 to 47 traces. This section should be

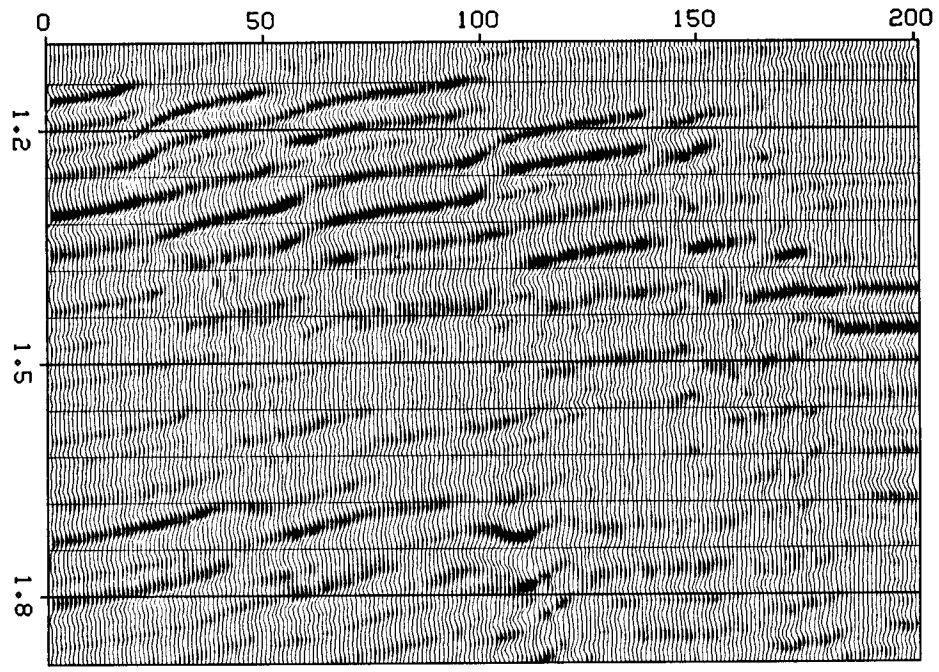

FIG. 4. Unmigrated, zero-offset stacked section of data from the Gulf of Mexico.

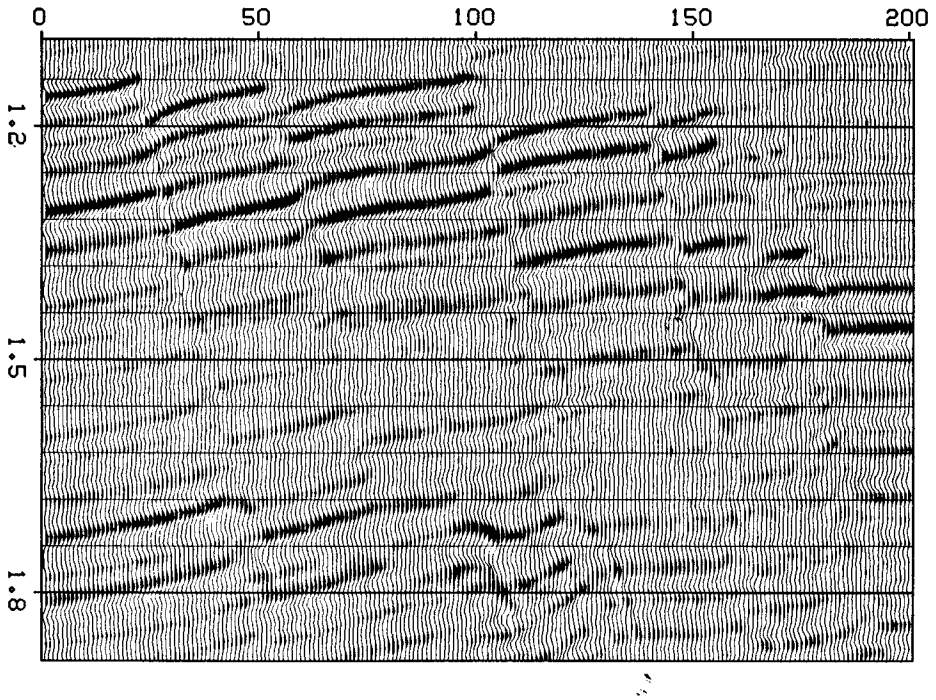

FIG. 5. Stolt migration of the data in Figure 4. The migration velocity used was 1600 m/sec. Note the slight, laterally variable mispositioning of the steep fault plane reflections.

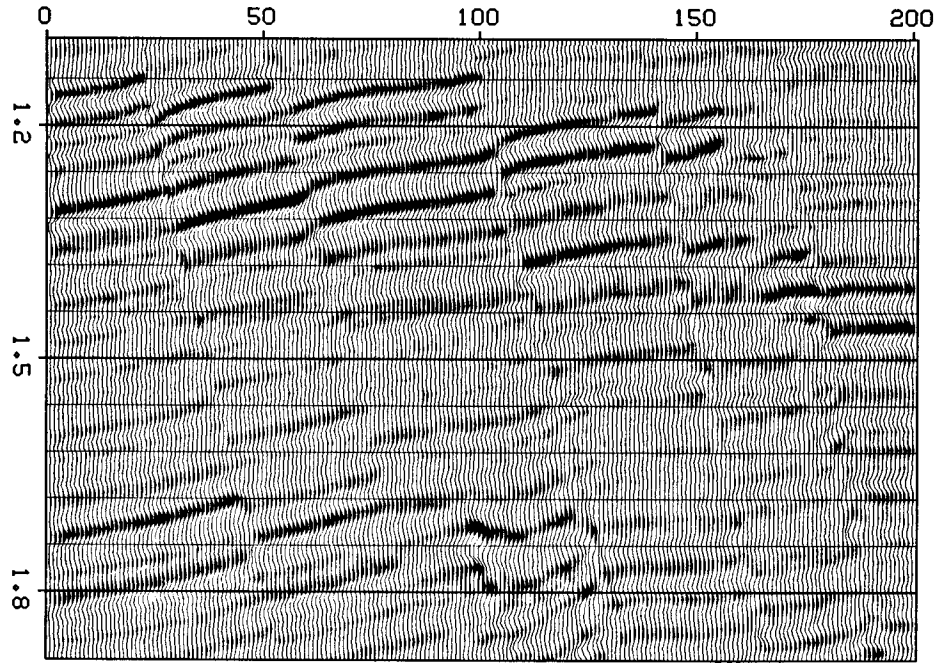

FIG. 6. Residual migration of the data in Figure 5. True migration velocities for the data range from 1650 to 2000 m/sec.

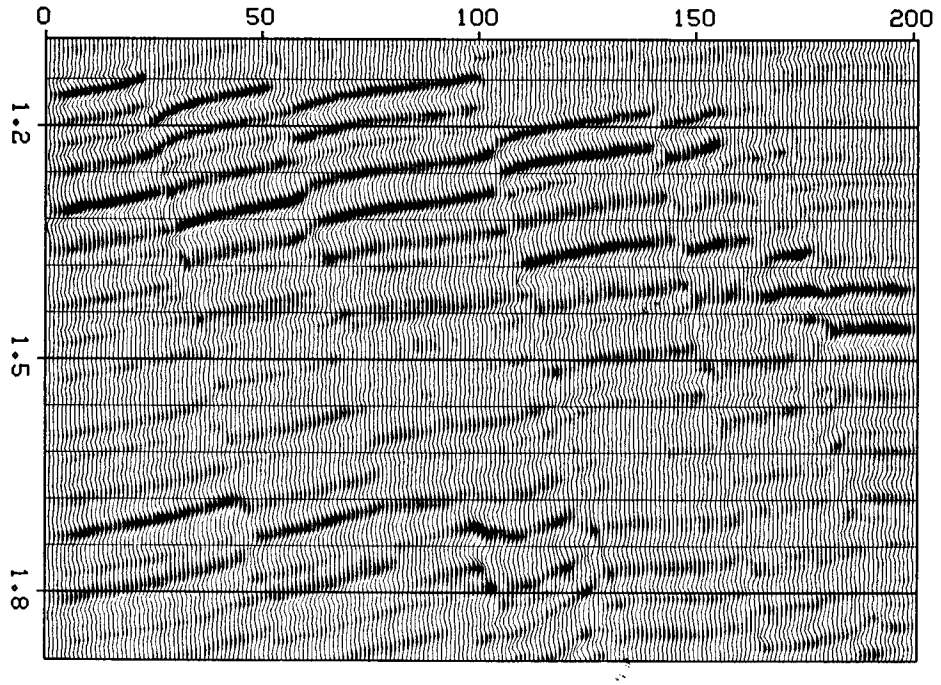

FIG. 7. Full Kirchhoff migration of the original data in Figure 4. The four-fold interpolation used prior to the migration in Figure 6 was also used here.

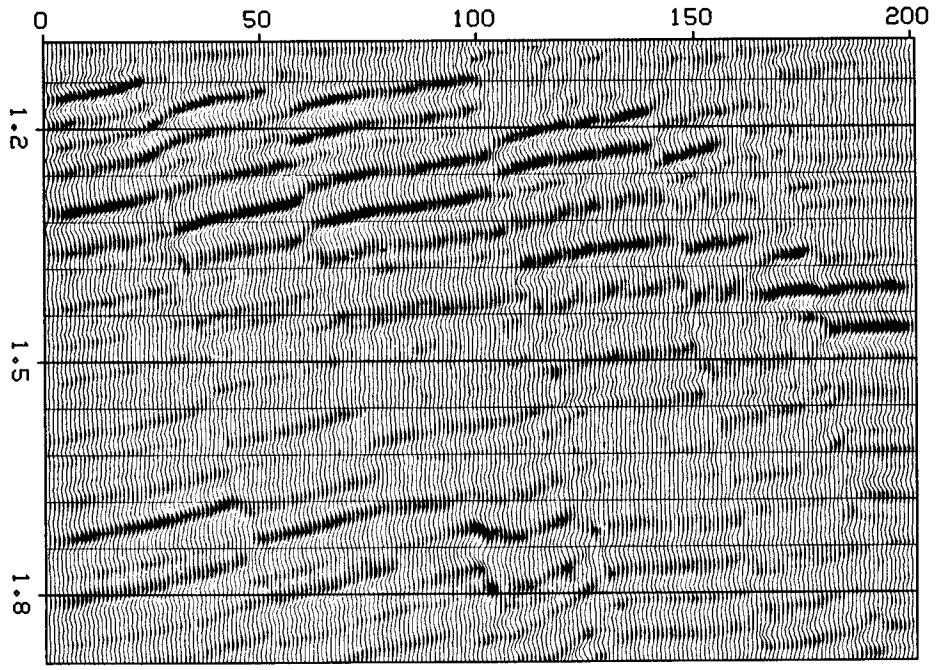

FIG. 8. Full Kirchhoff migration of the original data in Figure 4. No interpolation was performed.

compared with the equivalent residual migration in Figure 6. As expected, the two sections are virtually identical. The most discernible differences, however, occur at the sides of the data, arising from side truncations of operators of different lengths. For purposes of comparison, the same 4-fold interpolation used for the residual migration was used here. Full migration *without* any interpolation is displayed in Figure 8. The data are now contaminated by computational artifacts, especially at early times between traces 100 and 150. The poorest regions correspond to where the migration velocities varied strongly in the lateral direction. This full Kirchhoff migration, due to inadequate numerical integration as discussed in the previous section, was unable to properly handle the higher wavenumbers when velocity varied laterally. Thus, while interpolation may be a regrettable necessity for low velocity residual migration, it may also be desirable, as it was here, for ordinary migration.

Where now?

We have examined residual migration up to now as a tool for sharpening and fine tuning time migration and have gained some insight into its limitations. We still need to investigate the $v(z)$ issue. In particular, we expect that the user would prefer to apply residual migration to his best previous migration output rather than some constant velocity result. While the results of Gibson, Larner, and Levin (1983) on velocity error in 3-D migration give us a handle on what happens when migration velocity is to be changed by a constant factor, our simple example suggests we might encounter hidden pathologies when trying to modify the velocity field patch by patch.

A related issue is whether residual migration is the best tool for improving time migration. Dave Hale (private communication) argues that constant velocity scans using Stolt migration as presented by Chun and Jacewitz (1978) are at least as fast as residual migration. Dan Rothman takes a first look at this argument elsewhere in this volume in "A short note on constant velocity migrations."

Finally, we want to investigate residual *depth* migration. Heuristically, we have used residual migration to collapse small diffraction patterns resulting from velocity errors. From the viewpoint of Hatton, Larner, and Gibson (1981), we have split (and then separated) the *diffraction* term of the one-way scalar wave operator into two parts - the diffraction term for the first (incorrect) migration plus a residual error term. We have ignored, so far, the effect of velocity errors on the *thin-lens* term. Including this effect should lead to *residual image ray* correction. We are presently looking to the theory of *asymptotic rays* to unify the two corrections.

Conclusions

Residual migration is an efficient, wave-theoretically valid procedure when applied after an initial constant velocity migration. The effort expended by a preliminary migration substantially reduces the effective dip, velocity, and frequencies input to a residual migration.

The examples shown have demonstrated the practicality of this procedure. Numerical inaccuracies arising from very small residual velocities may be avoided, in the case of residual Kirchhoff migration, by spatial interpolation prior to low velocity diffraction summation. Although only instances of undermigration have been exhibited, overmigration may be corrected in much the same manner with a modeling algorithm. As discussed by Rocca and Salvador, residual migration may be applied to data that is both under- and overmigrated, first by migrating the lower half, then by modeling the upper portion.

ACKNOWLEDGMENTS

Appreciation is gratefully expressed to Dave Hale. His suggestions, criticism, computer programs, and data were especially helpful in the preparation of this report.

REFERENCES

Chun, J. and Jacewitz, C., 1978, A fast multivelocity function frequency domain migration, presented at the 48th meeting of the SEG, San Francisco.

Hale, D., 1982, Migration of non-zero-offset sections, SEP-30, p. 29-41.

Hatton, L., Larner, K.L. and Gibson, B.S., 1981, Migration of seismic data from inhomogeneous media, Geophysics, V. 46, p. 751-767.

Jakubowicz, H. and Levin, S., 1983, A simple exact method of 3-D migration - Theory, Geophysical Prospecting 31, p. 34-56.

Larner, K., Gibson, B., and Rothman, D., 1980, Trace interpolation and the design of seismic surveys, Presented at the 50th meeting of the SEG, Houston.

Rocca, F. and Salvador, L., 1982, Residual migration, Presented at the 52nd meeting of the SEG, Dallas.

Appendix

We show when residual migration is wave-theoretically exact. This is demonstrated for two cases; first, for constant velocity migrations, and then for constant velocity migration followed by residual migration in which velocity varies with depth.

Stolt migration of a wavefield $p(x,t,z=0)$ is performed by the mapping

$$k_\tau = \sqrt{\omega^2 - v^2 k_x^2} \tag{A1}$$

and the inverse Fourier transform

$$p(x,0,\tau) = \int\int P(k_x,\omega) e^{ik_x x - ik_\tau \tau} \left| \frac{d\omega}{d k_\tau} \right| dk_x \, dk_\tau \ . \tag{A2}$$

Assume that migration is instead performed with velocity $v_m \neq v$. The change of variable is now expressed as

$$\omega' = \sqrt{\omega^2 - v_m^2 k_x^2} \tag{A3}$$

and the partially migrated image is

$$p_1(x,0,\tau) = \int\int P(k_x,\omega) e^{ik_x x - i\omega' \tau} \left| \frac{d\omega}{d\omega'} \right| dk_x \, d\omega' \ . \tag{A4}$$

Migration is completed by the residual migration of p_1 with velocity $v_\varepsilon = \sqrt{v^2 - v_m^2}$. To do this, we define a new time section, $q(x,t,0) = p_1(x,0,\tau = t)$. The Stolt mapping we now use is

$$\begin{aligned} k_\tau &= \sqrt{\omega'^2 - v_\varepsilon^2 k_x^2} \\ &= \sqrt{\omega^2 - v^2 k_x^2} \ , \end{aligned} \tag{A5}$$

and the residually migrated image is

$$q(x,0,\tau) = \int\int Q(k_x,\omega') e^{ik_x x - ik_\tau \tau} \left| \frac{d\omega'}{dk_\tau} \right| dk_x \, dk_\tau \ . \tag{A6}$$

Substituting from equation (A4), the 2-dimensional Fourier transform of $q(x,t,0)$, we can then write

$$\begin{aligned} q(x,0,\tau) &= \int\int P(k_x,\omega) \left| \frac{d\omega}{d\omega'} \right| e^{ik_x x - ik_\tau \tau} \left| \frac{d\omega'}{dk_\tau} \right| dk_x \, dk_\tau \\ &= \int\int P(k_x,\omega) e^{ik_x x - ik_\tau \tau} \left| \frac{d\omega}{dk_\tau} \right| dk_x \, dk_\tau \end{aligned} \tag{A7}$$

This is the same integral as equation (A2), proving our assertion for constant velocity migrations.

For migration with depth variable velocity $v(z)$ we use the phase shift equation

$$p(x,0,\tau) = \int\int P(k_x,\omega) e^{ik_x x} e^{-i\int_0^\tau \sqrt{\omega^2 - v^2(\zeta)k_x^2}\, d\zeta} \, dk_x \, d\omega \ . \tag{A8}$$

If, instead, the Stolt migration described in equation (A4) is performed first, the output data, $q(x,t,0)$, may be residually migrated with velocity $v_\varepsilon(z) = \sqrt{v^2(z) - v_m^2}$ according to the formula

$$q(x,0,\tau) = \int\int Q(k_x,\omega') e^{ik_x x} e^{-i\int_0^\tau \sqrt{\omega'^2 - v_\varepsilon^2(\zeta)k_x^2}\, d\zeta} \, dk_x \, d\omega' \ . \tag{A9}$$

Replacing Q with P as we did in equation (A7), and also substituting ω for ω', we get

$$\begin{aligned} q(x,0,\tau) &= \int\int P(k_x,\omega) \left| \frac{d\omega}{d\omega'} \right| e^{ik_x x} e^{-i\int_0^\tau \sqrt{(\omega)^2 - v^2(\zeta)k_x^2}\, d\zeta} \, dk_x \, d\omega' \\ &= \int\int P(k_x,\omega) e^{ik_x x} e^{-i\int_0^\tau \sqrt{(\omega)^2 - v^2(\zeta)k_x^2}\, d\zeta} \, dk_x \, d\omega \ , \end{aligned} \tag{A10}$$

equivalent to expression (A8). Residual migration can thus be extended to depth variable velocity.

PERCEIVED QUALITY OF FACULTY IN GRADUATE PROGRAMS

	STANFORD RANKINGS				1982 RANKING (Standardized Score)						
HUMANITIES	**1957**	**1964**	**1969**	**1982**	**Berkeley**	**Harvard**	**Yale**	**Princeton**	**MIT**	**Chicago**	**UCLA**
Art History	NR	NS	11*	7 (59)	6 (64)	2 (69)	1 (75)	5 (66)	NL	13 (53)	12 (54)
Classics	15	NI	4	14 (55)	2 (67)	1 (70)	3 (65)	4 (62)	NL	10* (57)	16 (52)
English	15	6*	6*	10 (66)	2 (71)	4 (69)	1 (73)	7* (67)	NL	5* (68)	11* (64)
French	NR	11*	8	12 (59)	6 (61)	13 (56)	1 (74)	2 (73)	NL	13* (56)	31 (48)
German	NR	13*	5*	6* (63)	4 (65)	9 (59)	1* (67)	1* (67)	NL	21 (47)	11 (57)
Linguistics	NR	NI	Good	9 (58)	6* (61)	10 (55)	11* (52)	NL	1 (69)	4* (62)	2 (66)
Music	NR	NS	10*	14* (59)	1* (67)	NL	4 (66)	1* (67)	NL	1* (67)	11* (60)
Philosophy	NR	10	11*	7 (66)	4 (69)	1 (72)	14 (57)	2* (71)	9 (64)	6 (67)	5* (68)
Spanish	NR	NR	17*	7* (63)	5 (67)	1 (74)	3* (69)	13 (59)	NL	NL	7* (63)
SOCIAL SCIENCES											
Anthropology	14	10*	9*	7* (63)	1 (74)	7* (63)	6 (65)	37* (47)	NL	2* (73)	7* (63)
Economics	5*	6	7*	2* (72)	9* (65)	2* (72)	5* (71)	5* (71)	1 (73)	2* (72)	9* (65)
History	15	7*	5*	8 (67)	1* (71)	3* (70)	1* (71)	3* (70)	NL	5* (68)	10 (64)
Political Science	13	7*	6*	7* (66)	2* (71)	2* (71)	1 (72)	9* (63)	6 (67)	4* (70)	16 (59)
Psychology	5	1*	1	1 (72)	4* (69)	2* (70)	2* (70)	16* (63)	21* (62)	9* (67)	7* (68)
Sociology	NR	11*	15*	7* (66)	3* (69)	5* (67)	14* (62)	16* (60)	NL	1 (71)	8* (65)
Geography	(no program)				4* (66)	NL	NL	NL	NL	3 (67)	6 (64)
BIOLOGICAL SCIENCES											
Biochemistry	NS	2*	2*	1* (74)	4* (71)	1* (74)	7 (70)	25 (59)	1* (74)	15* (64)	12* (66)
Botany	14	9*	11	NL	3* (65)	NL	5 (63)	NL	NL	42 (45)	10* (60)
Cellular, Molecular	(new category)		4	11* (61)	8* (64)	6* (65)	4 (69)	28* (53)	1* (70)	11* (61) (C)	14 (60)
Microbiology	NS	7	8*	10 (64)	31* (56)	NL	13 (63)	NL	1 (77)	20* (61) (D)	8 (66)
Physiology	NS	24	Good	35* (54)	31 (55)	7 (65)	2* (68)	NL	NL	18* (58)	5* (67)
Zoology	14	4	3*	7* (66)	2 (70)	1 (74)	3* (69)	NL	NL	10 (62)	5* (67)
PHYSICAL SCIENCES											
Chemistry	15	5	3*	5* (70)	1* (74)	1* (74)	13* (64)	13* (64)	4 (73)	7* (69)	7* (69)
Computer Science	(new category)			1 (75)	4 (70)	NL	8 (60)	14 (55)	2 (74)	NL	6* (63)
Geoscience (A)	6	7	4*	5* (66)	9* (64)	7* (65)	9* (64)	7* (65)	2 (72)	5* (66)	3 (69)
Mathematics	9	6	6	6* (69)	2 (72)	3* (71)	6* (69)	1 (73)	2 (72)	4* (71)	14 (63)
Physics (B)	6	5	5*	6* (70)	3* (72)	1* (73)	11* (65)	3* (72)	3* (72)	6* (70)	17* (62)
Statistics, biostatistics	(new category)			1* (72)	1* (72)	6* (62)	13* (60)	6* (62)	NL	3 (70)	17 (59)
ENGINEERING											
Chemical	NS	10*	4*	5 (70)	3* (71)	NL	30* (50)	9* (64)	7 (67)	NL	35* (49)
Civil	NS	5	4*	5* (67)	1 (75)	NL	NL	10* (61)	2 (74)	NL	16* (58)
Electrical	NS	2	2	2* (75)	2* (75)	NL	30* (54)	10* (63)	1 (76)	NL	5* (67)
Mechanical	NS	3	2	2 (74)	3 (73)	NL	23* (54)	6 (66)	1 (76)	NL	9* (64)
	ranked first			4	5	7	6	3	6	2	0
	top 5			11	24	15	15	10	13	13	6
	top 10			25	30	22	20	18	16	18	17
	total fields			30	32	23	30	26	17	26	32
	fields in survey			32	32	32	32	32	32	32	32

* = *tie*

NL = not listed
NR = not ranked
NS = not surveyed
NI = not included

(A) = ranking shown is for geophysics, geology had a standardized score of 60, applied earth science 56
(B) = applied physics had a standardized score of 65, equivalent to an 11th-place tie
(C) = ranking shown is for genetics, biology had standardized score of 55, biophysics and theoretical biology, 58, developmental biology 54
(D) = ranking shown is for microbiology, immunology had standardized score of 57, virology 68